Available online at www.sciencedirect.com
ScienceDirect
C. R. Physique 7 (2006) 592–605
COMPTES RENDUS PHYSIQUE
http://france.elsevier.com/direct/COMREN/

Turbulent transport in fusion magnetised plasmas/Transport turbulent dans les plasmas magnétisés de fusion

Transport modelling

Arthur G. Peeters *, Clemente Angioni, Giovanni Tardini

Max Planck Institut für Plasmaphysik, Boltzmannstrasse 2, 85748 Garching bei München, Germany

Available online 1 September 2006

Abstract

Linear and quasi-linear transport models for core transport of a tokamak plasma are reviewed. The dependence of the modelled transport on the main plasma parameters is discussed. The comparison of the models with the experiment is reviewed both directly in terms of the predicted stored energy as well as indirectly discussing key physics ingredients of the models. ***To cite this article: A.G. Peeters et al., C. R. Physique 7 (2006).***

Résumé

Modélisation du transport. Cet article présente une revue des modèles linéaires et quasi-linéaires du transport dans les plasmas de coeur dans les tokamaks. La dépendance du transport en fonction des paramètres principaux est discutée. Ces modèles sont ensuite confrontés aux résultats expérimentaux par comparaison directe de leur prédiction en contenu énergétique, et aussi par analyse des leurs principaux ingrédients. ***Pour citer cet article : A.G. Peeters et al., C. R. Physique 7 (2006).***

Keywords: Plasma transport modelling; Tokamak plasma; Plasma parameters

Mots-clés : Modélisation du transport de plasma ; Plasma tokamak ; Paramètres des plasmas

1. Introduction

This article deals with (quasi-) linear transport models for the core (innermost 80% radius) of a tokamak plasma. It cannot be considered a proper review on the subject. Firstly, although references to other works are added, all the examples in the form of figures are taken from the work of the authors. Secondly, completeness of the referenced works is not claimed, and no attempt is made to properly represent all the (often different) opinions in this area of research.

The tokamak transport that is due to the combination of particle orbits in the (slowly varying) magnetic field and Coulomb collisions is referred to as neo-classical transport. This transport theory is well worked out and the fluxes can be readily calculated. Experiments, however, show a much higher level of transport which is referred to as anomalous. Neo-classical transport fluxes, although not always dominant, are nevertheless expected to exist in tokamak plasmas and in the modelling of temperature and density profiles they are often added to the modelled anomalous fluxes.

* Corresponding author.
E-mail address: arp@ipp.mpg.de (A.G. Peeters).

1631-0705/$ – see front matter
doi:10.1016/j.crhy.2006.07.011

Anomalous transport in tokamaks is expected to be due to turbulence. Several sets of model equations exist that describe the turbulent state, with the most accurate model being the gyro-kinetic description. There are many computer codes that solve one of these sets of non-linear equations. They can be used to obtain the fluxes of energy and particles as a function of the gradients and, in some cases, also the evolution of the temperature and density profiles.

When discussing 'Transport modelling' the fusion community, however, does not generally refer to this direct comparison between theory and experiment. Rather one refers to a comparison between experiment and somewhat more simplified models that try to capture (some of) the properties of the turbulent state. Such an approach is often necessary since the turbulence codes are computationally too demanding. In this paper only the results of the 'simplified' models will be reviewed. Simplified here means linear or quasi-linear, i.e., we will not consider models that evaluate the non-linear mode coupling explicitly.

Of course, as time progresses, computers become more and more powerful, and in fact direct comparisons between turbulence calculations and experiments are possible today for a limited amount of cases. It is clear that the modelling of transport will in the future be more and more dominated by non-linear models. It will also be discussed in the next section that the simplified models do indeed have serious limitations. This means that the research described in this article should, in the opinion of the authors, be directed more at a qualitative explanation rather than exact quantitative agreement. Linking experimental observations to elements in the theory implies that the result is of relevance even outside a particular model, and furthermore gives more reliability to the result (because it is not model specific). It is, therefore, our aim to identify key elements in the physics of transport and to determine to what extent these are reflected in real experiments.

This article is organised as follows. In Section 2 the different transport models and their physics contents is discussed. The main dependences of the predicted transport fluxes on plasma parameters are then shown and compared in Section 3. In this section it is also discussed how well the models reproduce the experimentally determined stored energy. Sections 4 to 8 then discuss the modelling results in terms of key physical elements: the threshold, stiffness, coupling of channels, and dimensionless parameters. Finally, conclusions are drawn in Section 9.

2. Transport models

Ideally a model is constructed with a certain set of assumptions and has an expected region of validity in terms of the parameter space. This model can then be compared with experiment and tested against it. Obviously it makes no sense to apply it outside its range of validity, and, when properly constructed, what one tests is the set of assumptions. A good model should have a reasonable range of applicability and should not make any assumptions that can, on theoretical grounds by a more complete description, be ruled out.

Transport models are far from ideal. In many cases the so-called quasi-linear theory is used. This theory calculates the transport fluxes using the linearly unstable eigenmodes of the system. Often only one mode is used, mostly the most unstable mode, but also averages over a spectrum of modes is applied in the literature. The saturation level of the unstable modes is calculated by balancing the linear drive of the instability with the non-linear terms that represent the mode coupling with itself. Turbulence simulations, in general, do not support this physical picture of the saturation. The turbulent state is better described by the non-linear interaction of many modes (both unstable as well as stable). The use of quasi-linear theory can therefore not be justified.

However, the quasi-linear theory leads to results that are to some extent applicable outside the region of its validity. The only proof of such a statement can, of course, be obtained comparing directly the non-linear results with the results from quasi-linear theory. Often a direct comparison of the fluxes for a given set of parameters gives a strong disagreement. However, it was, for instance, found in [1] that the scaling of the heat flux with plasma parameters obtained from non-linear calculations follows largely the quasi-linear predictions. In other words, a reasonable description of the simulated transport flux could be obtained if one re-scales the quasi-linear results with a constant factor. The reason for this could lie in the observation that for core turbulence the mode structures in the nonlinear phase are close to those of the linear phase. This is, for instance, for the Trapped Electron Mode (TEM) shown in [2]. The saturation might involve the interaction with more than one mode and, therefore, be inaccurately predicted by the quasi-linear theory, but the fact that the linear mode structure is more or less maintained makes that the linear properties of the instabilities are to some extent recovered in the non-linear phase. We note here that in this physics picture especially the relative transport in the different channels is expected to be well predicted by quasi-linear theory (the relative fluxes are independent of the saturation level). Linear stability seems much less relevant in the edge of

the plasma, where the nonlinear drift wave [3] plays an important role. Furthermore, in the edge of a reactor relevant discharge scenario one has to deal with the a so-called transport barrier which further complicates the description. For these reasons transport modelling is often applied only to the core of the plasma.

Of course, the discussion above is only a weak defence of the use of quasi-linear theory. In fact, no systematic study on the limits of its applicability exists, and there are many known cases in which nonlinear mechanisms enter and change the physics picture obtained. We will try to point out some of these effects when we discuss the results in the later sections, and we will also discuss agreement with nonlinear models if it is known to exist.

The quasi-linear model is not the only, though maybe the least tractable, approximation made in transport models. The motivation for further approximation often lies in computational resources. For the comparison between experiment and theory one can choose two slightly different approaches. One can try to simulate the hole profile through time integration of a transport model including the particle and heat sources, or one can use all the experimentally obtained information to calculate a local heat or particle flux for a given set of observed profile gradients. The first of these methods is generally more accurate. Gradients of profiles reconstructed from a finite number of local measurements are often not accurately determined. Unfortunately, the transport is very sensitive to the gradients such that a small error in the determination of the gradient can lead to a large discrepancy when comparing theory and experiment. The full integration of the profiles can be thought of as an averaging procedure over a larger radial domain, leading to more accurate results. On the other hand the local determination of the heat flux for a certain set of plasma parameters requires, when compared with the model, only one evaluation of the transport fluxes by the model calculations. This is less demanding in terms of computational recourses and allows more complicated models to be tested against the experiment.

The models that allow for a time integration of the full profile into steady state are based on fluid equations and, therefore, make a closure approximation. They also use a prescribed functional form of the mode structure in order to obtain a 0-dimensional dispersion relation. The geometry is furthermore approximated, and is based on circular shifted circles, the so called $\hat{s} - \alpha$ model (see [4–6] for a discussion on the influence of geometry). In principle the models mentioned above can also be used (and are in fact often used) for local comparisons. Such comparisons, however, can also be made using the gyro-kinetic equation in the ballooning approximation or even globally.

Below we will first briefly describe the fluid models based on the Ion Temperature Gradient (ITG), the Trapped Electron Mode (TEM) and (to a lesser extent) the Electron Temperature Gradient (ETG) mode. These are not the only transport models that are used in the community. The Current Diffusive Ballooning Mode (CDBM) [7] model for instance is based on the assumption of a different nonlinear instability dominating transport. We have chosen the ITG/TEM system since almost the entire nonlinear literature points at these modes being the main players in the determination of transport fluxes. Besides the theory motivated models a large number of empirical or semi-empirical models does exist. These models have an agreement with the experiment similar or better than the theoretical models [8], and are often excellent 'flight simulators'. The are not reviewed here, however, since they do not allow one to make a connection between observation and theory. Also since they do not have a strong physics basis such models are less suited for reliable extrapolations. Finally, several models have been constructed around modes that should dominate in the edge of the plasma. They are not reviewed here because we will concentrate on the core.

2.1. The Weiland model/multi-mode model

The Weiland model [9,10] is a fluid model that describes the ITG/TEM system. The fluid system is reduced to a 0D dispersion relation by assuming a fixed poloidal wave-vector $(k_\theta \rho_s)^2 = 0.1$ (where ρ_s is the ion Larmor radius calculated with the electron temperature) as well as a radial wave vector $k_r = k_\theta$. (Recently the model has been modified to include a variable poloidal wave vector but this does not apply to the results discussed in this paper.) The direction along the magnetic field is treated using the strong ballooning approximation [5]. Different versions of the model exist, with the most complete containing the effect of impurity dilution, electromagnetic effects, parallel ion motion, and finite Larmor radius effects in lowest order expansion.

As for all fluid approaches a closure approximation needs to be made. Weiland has explicitly chosen a non-dissipative closure scheme in which the higher moments that are not treated as dynamical variable, but are calculated using the Maxwell distribution. It is assumed that in the nonlinear state the dissipative terms that would be obtained linearly are no longer relevant [11].

The saturation of the mode is evaluated using the assumption that the growth of the mode is balanced by the main nonlinearity

$$\gamma \widetilde{T} = \mathbf{v}_E \cdot \nabla \widetilde{T} \tag{1}$$

where γ is the growth rate, $\widetilde{T}$ is the temperature perturbation, and $\mathbf{v}_E$ is the $E \times B$ velocity. This leads to a saturated electro-static potential (ϕ)

$$\frac{e\phi}{T_e} = \frac{\gamma/\omega_{ci}}{k_r \rho_s k_y \rho_s} \tag{2}$$

which in turn leads to a heat transport coefficient (χ) proportional to

$$\chi \propto \frac{\gamma^3/k_\theta^2}{(\omega - 5/3\omega_D)^2 + \gamma^2} \tag{3}$$

where ω is the real frequency of the mode, and ω_D is the drift frequency. Note that this relation is nonlinear in the growth rate of the mode as long as the growth rate is smaller than the real frequency.

The multi-mode model [12,13] can be seen as an extension of the Weiland model. It uses the Weiland model, but adds the effects of drift-resistive and kinetic ballooning modes.

2.2. The GLF23 model

The GLF23 (Gyro Landau Fluid) model [14] is also based on a 0D dispersion relation obtained from fluid equations. The starting point, however, is the gyro-fluid equations and dissipative terms in the form of collisions and Landau damping are kept. The latter are modelled by adding terms in the pressure and parallel momentum equations with arbitrary constants. These constants are then adjusted such that the model matches the predictions of linear gyro-kinetic simulations (with GKS [15]). Besides the above mentioned constants other parameters (the dependence of the radial component of the wave vector on the poloidal wave vector and magnetic shear for instance) are adjusted in the matching procedure. Finally, the overall level of transport is adjusted using one constant to match the results of nonlinear gyro fluid simulations. More recently, [16], the latter coefficient has been adjusted to match the more accurate nonlinear gyro-kinetic simulations made with the GYRO code [17]. It is important to stress that the matching procedure uses theoretical results and that experiments play no role in the construction of the model.

The model consists of 8 equations for the ion density, the parallel and perpendicular pressure of the ions, the density and both pressures for the trapped electrons, the density of the passing electrons, the parallel component of the vector potential and the quasi-neutrality equation. The effect of impurities can be treated assuming they dilute the main ion species. These equations describe the ion temperature gradient mode, the collisionless as well as dissipative trapped electron mode, ideal MHD ballooning modes as well as resistive modes that play a role in the edge. Electron Temperature Gradient modes can be described through their symmetry with respect to ITGs.

Like the Weiland model the dimensionality is reduced using a wave vector representation perpendicular to the magnetic field. Again the radial and poloidal wave vector are taken to be equal. Along the magnetic field the model is based on a Gaussian test function with a width that is mainly a function of the safety factor and the magnetic shear. The model uses 10 different values of the poloidal wave number and calculates the quasi-linear fluxes through a summation over all the unstable modes. The saturation amplitude is calculated for each mode individually, and follows a mixing rule which gives for the heat conduction coefficient

$$\chi = \frac{3}{2}\frac{\gamma}{k_r^2}\frac{\gamma\gamma_d}{\gamma^2 + \omega^2} \tag{4}$$

where γ is the growth rate , γ_d is the damping rate of a representative radial mode (which is taken to be proportional to the drift frequency), and ω is the real frequency. Besides the particle flux and the electron and ion heat fluxes the model also provides the flux of toroidal momentum.

2.3. The IFS-PPPL model

A slightly different strategy than that described above was used in the construction of the IFS-PPPL model. The authors of this model realised the importance of the threshold behaviour of the instabilities with respect to the gradients. A large number of linear gyro-kinetic simulations were performed to determine this threshold accurately.

Non-linear gyro-fluid simulations were then used to determine the scaling of transport above the threshold. The model as constructed only deals with the Ion Temperature Gradient mode. The electron heat transport coefficient is estimated using a quasi-linear model, but a transition to the TEM can not be described. Neither is there a description of particle transport. The above mentioned limitations mean that this model is no longer widely used.

2.4. Local gyro-kinetic models

The local comparisons often use the gyro-kinetic model. Several codes exist that solve the linear gyro-kinetic problem either locally or globally [15,18–21]. Since the gyro-kinetic model is more complete it plays a special role in checking the results of the fluid models, calibrating the fluid model (as in the case of GLF23), or even largely determine the transport model as is the case in IFS-PPPL. Although our emphasis is on the fluid models, we will discuss some results of linear gyro-kinetic theory.

2.5. Shear flow stabilisation

Sheared plasma flows can stabilise turbulence. All models implement this stabilisation, the $E \times B$ shear, in the same way based on the simple criterion of stabilisation [22,23]. The shearing rate $\omega_{E\times B}$ is simply subtracted from the growth rate of the instability to obtain a new 'net' growth rate which is then used in the quasi-linear expressions. $E \times B$ shear stabilisation plays an important role in barrier formation which will be discussed in a separate paper [24].

3. Comparison between the models

In this section the main parameter dependence of the models are discussed and compared. After that we will compare and discuss which of the models describes best the stored energy of the plasma.

3.1. Main dependence within the models

A quantitative comparison between the transport models and the experiments is not conclusive for judging whether a model is correct. It is also important to determine if the transport model has a correct dependence on the relevant physical parameters. For this reason in this section the dependence of the models on physics parameters is shown, and the different models are compared. The only link to the experiment is that the two standard sets of plasma parameters are chosen to have values of a typical NBI (Neutral Beam Injection) heated discharge at mid radius and a typical ECH (Electron cyclotron heating) discharge again at mid radius of the ASDEX Upgrade tokamak. Each parameter in the standard set is then varied separately while keeping the others constant. The two standard sets of background parameters are presented in Table 1. Given the respective values of n_e and T_e, the collisionality in the two discharges is roughly the same and fairly low. Although the IFS/PPPL, GLF23 and Weiland models are based on the same instabilities, they yield different transport predictions due to the different approaches and approximations. In the Weiland model, the collisions on trapped electrons are switched off, in agreement with the most common use of this model in the literature. The stabilising effect of $\omega_{E\times B}$ has been neglected for all models, in order to distinguish more clearly the physics effects within the models. The ITG/TEM models are primarily sensitive to R/L_{T_i}, R/L_{T_e}, R/L_{n_e}, the safety factor q, $\hat{s}$, the effective ion charge Z_{eff}, the ratio T_e/T_i and the temperature values.

First the dependence of the transport on the gradients are analysed. Fig. 1(a) illustrates the different behaviours of the ITG in the models: the Weiland and GLF23 models have a similar ITG stability threshold around $R/L_{T_i} = 4$, IFS/PPPL somewhat lower. However, the GLF23 model has significant residual transport even for flat T_i profiles, due

Table 1
Background parameters for the stand-alone runs of the models

Shot	R/L_{T_i}	R/L_{T_e}	R/L_{n_e}	q	$\hat{s}$	Z_{eff}	T_i	T_e/T_i	n_e
13 042	7.4	5.3	3.2	1.8	0.9	1.1	3.4	0.8	3.7
13 558	*2*	9.1	0.4	1.7	0.9	1.1	*0.7*	3.2	2.0

T_i is not measured for # 13558. The arbitrary values $T_i = 0.7$, $R/L_{T_i} = 2$ are taken.

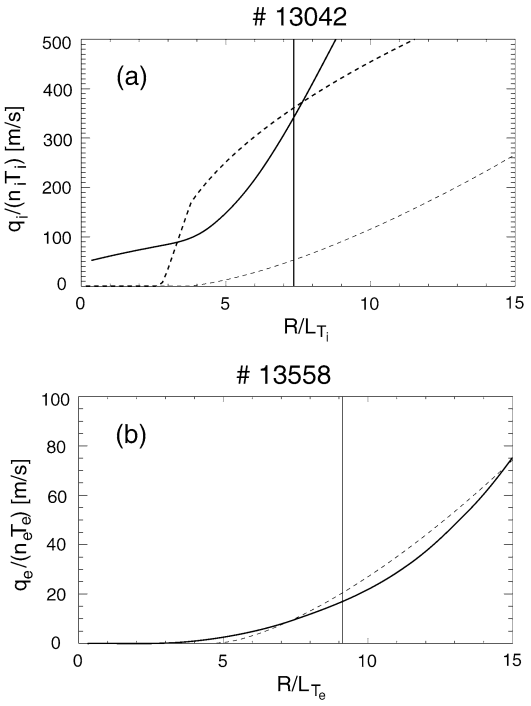

Fig. 1. Dependence of the heat fluxes on the inverse temperature gradient lengths according to the GLF23 (solid line), Weiland (thin dashed line) and IFS/PPPL (thick dashed line) models. (a) Ion heat flux versus ion temperature gradient, background parameters from Table 1, first row. (b) Electron heat flux versus electron temperature gradient, background parameters from Table 1, second row. The vertical line represents the experimental value of the scanned quantity as reported in Table 1. The IFS/PPPL model is not plotted in (b) because it does not depend on R/L_{T_e}.

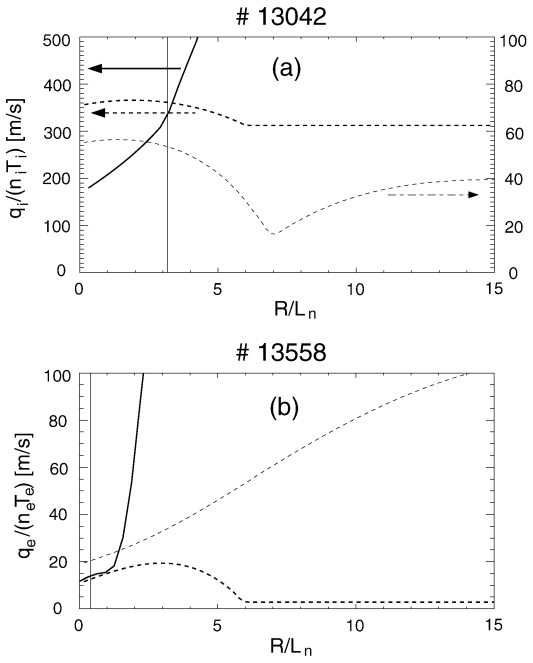

Fig. 2. Ion (a) and electron (b) heat flux versus the density gradient length. Lines and background parameters as in Fig. 1. Notice the different scale for the Weiland model output.

to the high density gradient (see also Fig. 2). The GLF23 and IFS/PPPL models exhibit a steep increase of transport above the threshold, whereas the Weiland model returns a smoother growth. This increase determines the stiffness of the profile and will be further discussed in one of the sections below. It is important to note here though that the version of GLF23 used is the original version, not the re-calibrated one based on GYRO simulations. In the latter the fluxes are roughly 4 times smaller. In Fig. 1(b) the IFS/PPPL model is not shown since it has no explicit dependence on R/L_{T_e}. The GLF23 and Weiland model exhibit similar behaviour and do not predict a strong T_e profile stiffness, as the heat flux increases smoothly above the critical threshold. However, there are significant differences between the models.

Fig. 2 illustrates the impact of the density gradient on transport. Both the ion as well as the electron density gradient length are varied, keeping $L_{n_i} = L_{n_e}$ in order to preserve quasi-neutrality. While the IFS-PPPL and Weiland models react weakly to density gradient changes, GLF23 is affected dramatically in both cases. This dependence can in fact be considered too strong, and makes that one needs to be careful with simulations using the GLF23 model and fixed density profiles. If the prescribed density profile is too peaked the predicted temperature profiles will have zero gradient. The IFS-PPPL formulas for χ's are not constructed for $R/L_{n_e} > 6$. Therefore, for steeper density gradients, no influence on heat transport is assumed and the model is not expected to reproduce the temperature profiles.

Another important parameter for the ITG turbulence is the ratio $\tau = T_e/T_i$; its direct impact on transport can be investigated varying it artificially, keeping constant both T_i and T_e. Instead, we report in Fig. 3 the experiment-relevant scans, where either T_i (a) or T_e (b) are varied. The temperature values strongly affect transport, determining to which extent the temperature profiles are expected to be stiff, as the models contain a $T^{1.5}$ dependence before the transport coefficients—the Gyro-Bohm factor. Notice that the temperature gradient lengths are kept fixed to the value reported

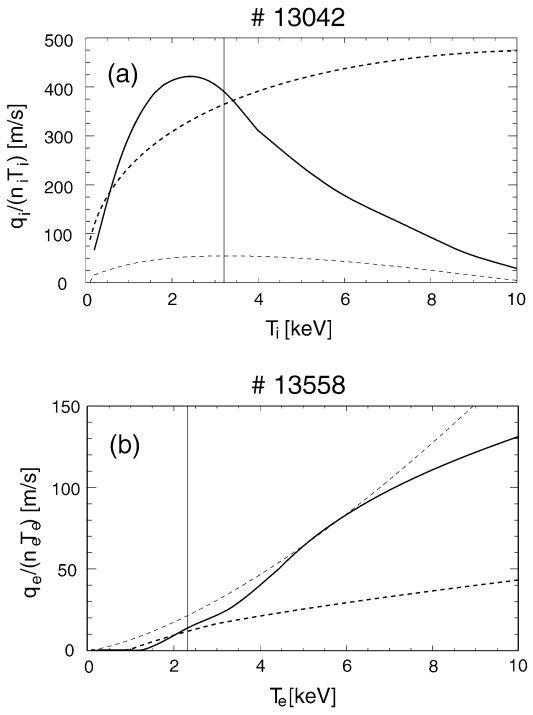

Fig. 3. Dependence of the ITG models on the temperature. (a) Ion heat flux versus T_i. (b) Electron heat flux versus T_e. Lines and background parameters as in Fig. 1.

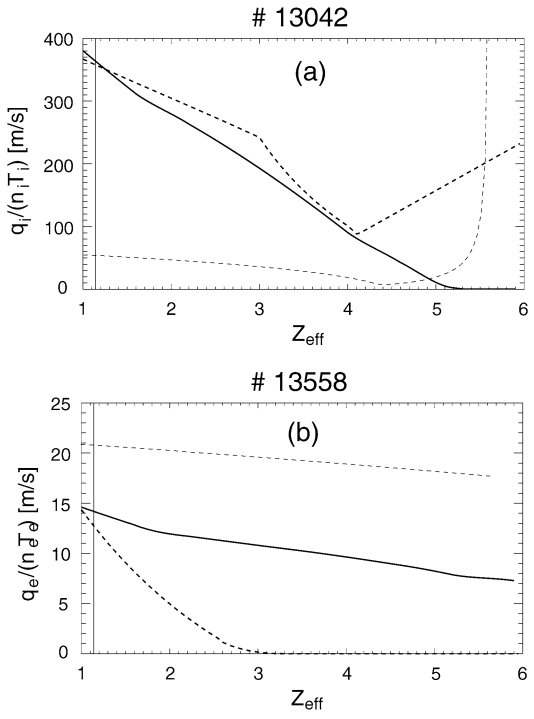

Fig. 4. Ion (a) and electron (b) heat flux versus the effective ion charge. Lines and background parameters as in Fig. 1.

in Table 1. For the ion case, both the Weiland and GLF23 models reach a maximum destabilisation of the mode when T_i equals T_e and then bend to a lower transport level; the IFS/PPPL model predicts the turbulent flux to increase monotonically with T_i. Hot electron temperatures enhance the TEM turbulence according to all models.

Also impurities can lead to different results, as illustrated in Fig. 4. In fact, impurities can be treated differently within one model. The GLF23 model, for instance, has a version with 8 equations (the one used for this comparison) in which impurities enter only as dilution and a version with 12 equations that retain the impurity dynamics. IFS-PPPL retains carbon as the main impurity, and a transition from the deuterium ITG to the carbon ITG can be observed for increasing Z_{eff}. For the TEM mode (see Fig. 4(b)) Z_{eff} has a weak effect. (The flux in the IFS-PPPL model is due to the ITG.)

Finally we report the dependence on the safety factor q (Fig. 5) and the magnetic shear (Fig. 6). The Weiland model depends very weakly on q, which in the core plasma ranges between 1 and 4; most probably the assumption for the parallel mode structure is too simplified. In general, q is observed to raise the turbulence level both theoretically [2] as well experimentally [25]. The IFS/PPPL formulas for χ's are not tested for low and negative shear, below 0.5, as reported by the authors [1]. The Weiland model assumes a dependence only on $|\hat{s}|$, a strong approximation which makes the model inadequate to describe negative shear scenarios. In addition, the dependence on $\hat{s}$ is observed to be linear. The GLF23 model has a more accurate description, with good overlapping with the IFS/PPPL model in the validity range of the latter. The magnetic shear is found to stabilise the turbulence for high as well as negative values.

3.2. Stored energy

The most direct quantity that can be predicted with the help of the transport models is the stored energy. This comparison has been done for various machines [8,26,16]. Shown in Fig. 7 is the simulated stored energy over the experimentally determined stored energy as a function of the boundary temperature (from [26]). Here the pedestal energy is subtracted to have a more precise comparison (because of the boundary condition the pedestal energy is always automatically recovered by the simulation; note too that it is up to 50% of the stored energy). The stored

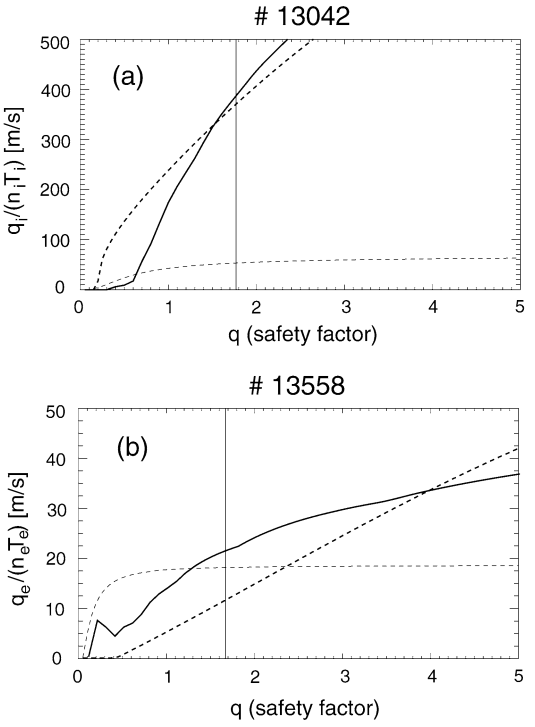

Fig. 5. Ion (a) and electron (b) heat flux versus the safety factor q. Lines and background parameters as in Fig. 1.

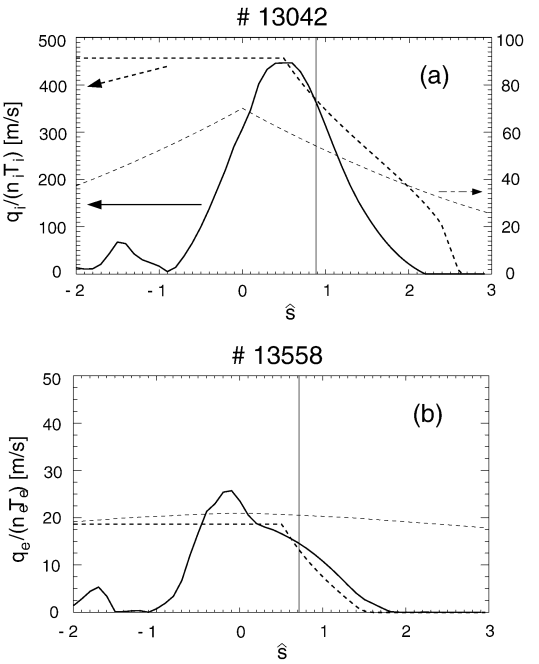

Fig. 6. Ion (a) and electron (b) heat flux versus the magnetic shear $\hat{s}$. Lines and background parameters as in Fig. 1.

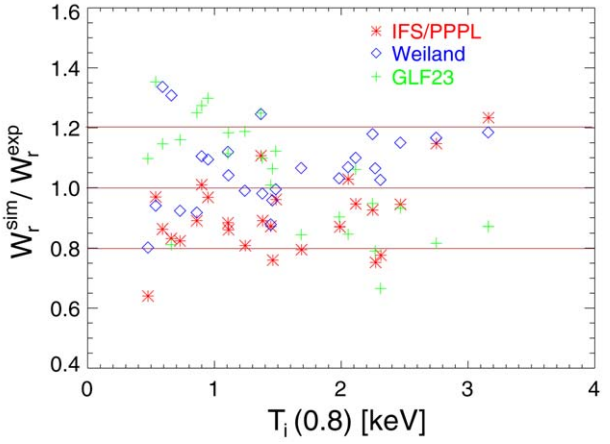

Fig. 7. Simulated stored energy over the experimentally determined stored energy (pedestal energy subtracted) for a set of ASDEX Upgrade discharges.

energy is predicted with an accuracy of roughly 15%. This is roughly as good as the scaling laws, and also in the range of the measurement errors. Comparisons have also been made with modulated experiments. Here it was found that GLF23 and IFS-PPPL tend to give better agreement for the ion temperature [27] whereas the Weiland model gives somewhat better agreement with the electron temperature [27,28]

Although the agreement with experiments is satisfactory, the comparison between theory and experiment is disappointing in the fact that it almost does not allow one to distinguish between the models. Models with quite different parameter dependence lead to similar results. The experimental variation in parameters is often small, or different parameters are too strongly correlated to come to clear results.

4. The threshold

The importance of the threshold has first been discussed in relation with the ion heat transport. It was mostly the work reported in [1] that demonstrated the importance of the threshold. In this reference the IFS-PPPL model (see previous section) was introduced and compared with results from TFTR, with good agreement being found.

Here the threshold will be discussed for the case of dominant electron heating, for which the dominant mode is expected to be a trapped electron mode. This is done solely because there exist better measurements of the electron heat flux versus the normalised electron temperature gradient when compared with the measurements of the ion temperature. For ion temperature profiles one has to consider the threshold together with the concept of stiffness which is discussed in the next section.

Fig. 8 from [29] shows the result of a local comparison between experiments and quasi-linear GS2 calculations. Shown is the electron heat flux as a function of the normalised gradient. These experiments have been specially designed to vary the electron heat flux at nearly constant electron temperature [30]. In this way the effect of T_e and R/L_{T_e} can be separated. It can be seen that the data shows a nearly linear relation between the electron heat flux and the normalised temperature gradient length R/L_{T_e}. A linear fit would clearly cross the $q_e = 0$ line at finite R/L_{T_e}. The value of R/L_{T_e} at the crossing is the experimentally determined threshold, and is interpreted to be related with the theoretical threshold of the trapped electron mode. It must be noted that experimentally one observes a very low level of transport below the threshold [31] which is interpreted to be due to an instability different than the TEM.

From the comparison with the GS2 quasi-linear results it is clear that the theory describes very well the behaviour of the electron heat flux. It should be mentioned here that an arbitrary factor is used to scale the calculations on top of the measurements such that one should only compare the shape of the curves (this arbitrary scaling factor is in agreement with the statements on the accuracy of quasi-linear theory made above). Nevertheless, the off-set linear scaling of the heat flux is nicely reproduced by the theory. At low values of the electron heat flux, the flux is not linear in the gradient of the electron temperature. This is due to the density gradient drive. At higher density gradient, the electron heat flux never goes to zero but has a shape similar to the dotted line (which here is the heat flux calculated for the same density gradient but without collisions). The experiments have a rather inaccurately determined density gradient ($\pm 20\%$) which has a value close to the point were the electron heat flux no longer goes to zero. It should be noted here that non-linear gyro-kinetic simulations [2,32] largely confirm the picture above, but do yield different results for sufficiently large density gradients. At larger values of R/L_N the threshold that is found when extrapolating the electron heat flux towards zero is no longer a strong function of the density gradient.

The existence of the threshold for the electron heat transport is not necessarily a generally accepted experimental fact. Results on DIII-D are not conclusive [33]. Tore Supra on the other hand finds a clear threshold [34] which, however, is not attributed to the TEM, but to the electron temperature gradient (ETG) mode [35]. More information on electron heat transport can also be found in [36].

5. Stiffness

It can be seen in Fig. 8 that for the discharges with dominant electron heating the threshold can be exceeded by a factor up to 2. Since the experiments are done with a certain amount of heating power, such a factor is determined by the steepness of the q_e versus R/L_{T_e} curve. A strong increase of q_e leads to a so-called stiff profile, i.e., a profile that has a gradient length close to the threshold independent of the amount of heating power applied. Since the threshold can be exceeded by a factor roughly 2 for the electrons, one sometimes speaks of a 'moderately' stiff profile.

A stronger stiffness is found to exist for ions. In fact the role of the threshold was first discussed in combination with stiff ion temperature profiles in [1], and is the essential basis of the IFS-PPPL model. In [1] the stiffness of the ion temperature profiles is demonstrated using TFTR data. Later papers have shown the ion temperature stiffness to exist also on ASDEX Upgrade [37] and JET [38]. Fig. 9 shows a graphical representation of the stiff profiles developed in [37]. For profiles that have a constant logarithmic gradient the central temperature is proportional to the temperature at the edge. In a plot of the central against the edge temperature the points should therefore line up on a straight line through the origin, whereas for the case with constant χ the points should also line up on a line which, however, does not cross the origin. It is clear from the figure that the data of ASDEX Upgrade supports the assumption of stiffness, although the amount of stiffness is not directly determined.

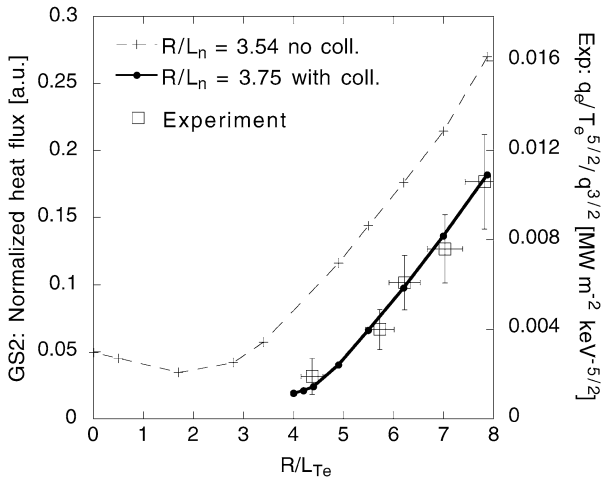

Fig. 8. Comparison of the experimental electron heat flux as a function of R/L_{T_e} with the results of quasi-linear theory.

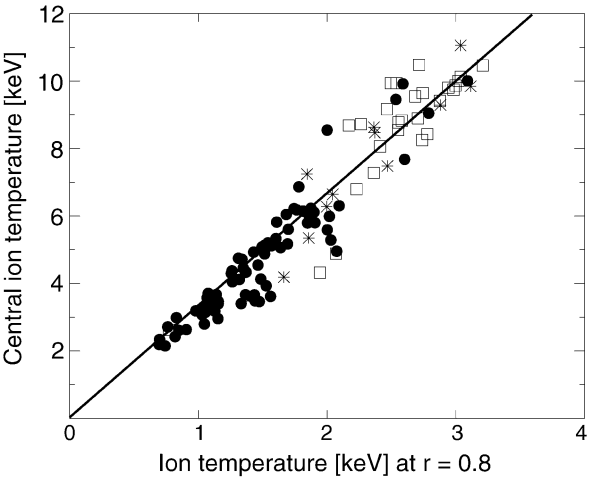

Fig. 9. Central ion temperature as a function of edge temperature for various discharges of ASDEX Upgrade.

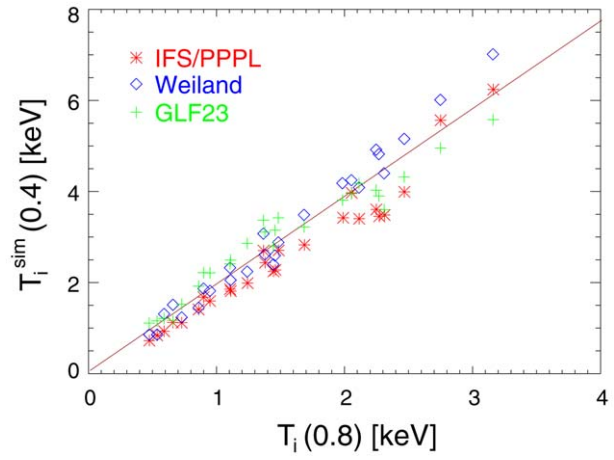

Fig. 10. Ion temperature at the normalised toroidal flux radius $\rho_t = 0.4$ as a function of the value at $\rho_t = 0.8$ calculated by the various transport models.

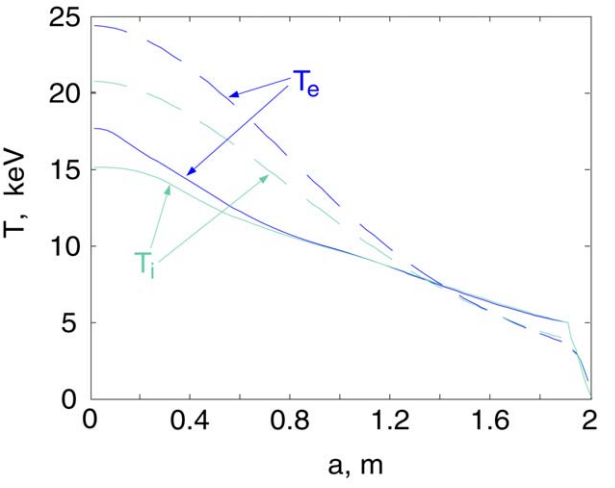

Fig. 11. Temperature profiles of an ITER simulation with GLF23.

A measure of the stiffness can be given by the quantity

$$\chi_s = \frac{R}{nT}\frac{\partial q}{\partial R/L_T} \tag{5}$$

Usual tokamak plasmas have heat diffusion coefficients of the order of several m^2/s. Therefore $\chi_s > 10\ \mathrm{m}^2/\mathrm{s}$ refers to a relatively stiff profile.

The stiffness can be estimated on the basis of non-linear simulations. If one assumes that the ion heat flux is a linear function of the ion temperature gradient, as in fact demonstrated in [39], then the simulations presented in [40] (based on the LLNL gyro-kinetic code) and [41] (based on the GYRO code [17]) lead to the following rough prediction

$$\chi = \chi_s\left[1 - \frac{L_T}{L_{T\,\mathrm{crit}}}\right] \quad \text{with } \chi_s = 241\frac{T_k^{3/2}}{B^2 R} \tag{6}$$

where T_k is the temperature in keV, B the magnetic field in T and R the major radius in m. A standard discharge on AUG ($B = 2.5$ T, $T = 1$ keV, $R = 1.65$) would have $\chi_s = 23$ m^2/s. Or in other words if the applied heat flux is such that if $\chi \approx 2.5$ m^2/s then $1/L_T = 1.121/L_{T\text{crit}}$, i.e., the threshold is only exceeded by some 12%.

Fig. 10 shows a set of simulations of ASDEX Upgrade discharges with different transport models. The line in the figure represents roughly the experimental scaling. It can be seen that all models reproduce the experiment relatively well. This is despite the difference in stiffness with χ_s being an order of magnitude different between IFS-PPPL and Weiland. At present the data can be said to be in agreement with the thesis of stiff ion temperature profiles. However, an accurate experimental determination of the stiffness of the ion temperature profiles is still to be made.

It can also be seen in Fig. 10, that except for the two points with the highest edge temperature, the IFS PPPL model systematically under-predicts the ion temperature at $\rho_{\text{tor}} = 0.4$. Since it is this model that incorporates most accurately the threshold it can be said that the experimental inverse temperature gradient length is found to be somewhat larger than the linear threshold. A stiffness that is smaller than the one found in nonlinear simulations could explain such a result, but also the so called Dimits shift [40] which is a nonlinear upshift ($\Delta(R/L_T) \approx 2$) of the threshold of the mode. In fact comparisons between IFS-PPPL and gyro-kinetic simulations have shown that IFS-PPPL should under-predict R/L_{Ti} by roughly 20% [40].

6. Coupling of channels

In general, an instability is driven by more than one gradient, and it leads to transport in more than one channel. This then leads to a complicated behaviour in which the relaxation of the different gradients is strongly coupled. The stationary state is determined by that set of gradients for which all the fluxes are balanced by the corresponding sources. Changing one of the sources might lead to (unexpected) changes in all the gradients, which are sometimes difficult to unravel. Of particular interest are those cases in which the flux moves up the gradient. It is clear from entropy arguments that such a process is only possible if the process that generates such a flux at the same time generates a flux in another channel which is directed down the gradient, and if the entropy production of the latter channel is larger than the negative entropy production of the former. (For a discussion on entropy production see [42].) The modelling of fluxes that are up the gradient has been discussed explicitly for heat transport [43] but there is an inward pinch for particle transport as well [44,11,54–56].

The picture above simplifies somewhat if one of the gradients provides the dominant drive. This generally means that also the flux in the channel that corresponds to the dominant driving gradient is larger than all other fluxes. When one gradient dominates it is this gradient that determines the growth rate of the mode, and the saturated amplitude of the fluctuating potential. The other gradients will still influence the magnitude of the fluctuating quantities corresponding with that gradient, but no longer the magnitude of the potential or even the phase shift between potential and fluctuating quantity. For the non-dominant channel the transport flux is (offset) linear in the corresponding gradient, with the flux for a given gradient being proportional to the flux in the dominant channel.

An example of the process discussed above is the ITG, which is dominantly driven by the ion temperature gradient, and not strongly effected by the gradients of density and electron temperature (provided both are sufficiently small). Under conditions of dominant ion heating the electron temperature gradient then decreases with decreasing electron heating or with increased ion heating [26]. Also density transport should increase with increased ion heating. Other good examples of such a coupling of channels are impurities and toroidal momentum [57,58]. The former is especially true when the impurity density is small, i.e., in the trace limit where the impurity density does not contribute in the quasi-neutrality equation as explicitly shown in [41,45]. The latter is because in general the energy carried by the toroidal momentum is much smaller than the thermal energy such that the momentum gradient does not strongly affect the growth rate of the mode [58]. The coupling between heat and momentum transport has been observed experimentally.

7. Dimensionless parameters

There are many investigations into the dependence of confinement on dimensionless parameters. These studies are mostly empirical. In terms of the confinement models, however, these dimensionless parameters represent clear physics ingredients, which will be discussed briefly in this section. There are, in essence, 3 dimensionless parameters: the normalised Larmor radius $\rho^* = \rho/a$, the normalised collision frequency ν^*, and the normalised pressure β.

7.1. Normalised Larmor radius

All the models that are discussed in this article are local on a certain flux surface. The gradients across the flux surface play a role but the models have no knowledge of the entire profile. These local models have the property that the normalised equations do not depend on the Larmor radius. One can therefore derive a perfect gyro-Bohm scaling

$$\frac{\chi}{B} \propto \rho_*^3 f(\nu_*, \beta, q, \hat{s}, \ldots) \tag{7}$$

An exception is given by the diamagnetic shear stabilisation in the GLF23 model [46,14], which leads to the breaking of the gyro-Bohm scaling [47], but this effect is often switched off in the simulations. Although the equation above seems to imply that perfect gyro-Bohm scaling must naturally follow from any transport simulation, this is not the case. The strong stiffness, for instance, can make the effective heat diffusion coefficient appear to scale differently. This can be understood if one assume a infinitely stiff system for both core as well as the edge. Doubling the power in such a system changes on χ by a factor 2, whereas ρ_* stays the same. Also imagine that the core shows a stiff behaviour but the edge of the plasma does not. In this case χ will reflect the scaling of the edge [48]. Small imperfections in the experiments, profile effects, and marginality have been found to explain the deviations from Gyro-Bohm scaling of the experiments [48,49,13].

7.2. Collisionality

The core of the tokamak is collisionless in the sense that the particles go around the device many times within one collision time. This is expressed in the value of ν^* being smaller than 1, where ν^* is the collisional de-trapping time normalised to the bounce time. Nevertheless, the collision time is not necessarily small compared to the real frequency or the growth rate of the instability. Collisions can therefore have an effect.

Because of their higher collision frequency the electrons are more affected by the collisions than the ions. In fact, since the ITG and TEM have frequencies of the order of the transit time of the ions, the small ν^* makes that the ion collision frequency is also small compared to the frequency of the wave, and can in fact be neglected. The electrons, on the other hand, have a collision frequency which is larger compared with that of the ions by the root of their mass ratio ($\sqrt{m_i/m_e}$). This collision frequency is not necessarily small compared with the wave frequency or growth rate. A good measure of the influence of collisions is the electron collision frequency normalised with the drift frequency $\nu_{\text{eff}} = \nu_e/\omega_D$ as defined in [50,51].

As can be expected the electron collisions mainly act through the de-trapping of trapped electrons, eliminating perturbations in the electron temperature inside the flux surface as well as density perturbations as far as they are non-adiabatic. In the presence of collisions the electrons can be expected to be more adiabatic. This reduces the growth rate of the trapped electron mode, but can also change the fluxes of the electron channel in the case of the ITG.

In the theory collisions have an important effect on particle transport. For an electro-static system the non-adiabatic electron response is mostly due to the trapped electrons. In the collisionless system the quasi-linear particle flux can be split in a diffusive contribution and a pinch velocity. The latter has a contribution due to the temperature gradient (thermo-diffusion) and due to the compression (curvature pinch). Nonlinear simulations [54,41] confirm this picture. It is the non-adiabatic response that can lead to a particle flux, and therefore collisions which reduce the trapped particle perturbations reduce the particle flux [50,51].

Experimentally a correlation between the density peaking and the collisionality is found [51,52]. With the peaking decreasing with increasing collision frequency. This behaviour can be well reproduced by the GLF23 model [50]. Unfortunately, it appears that in this point the model is not in agreement with gyro-kinetic simulations which also predict a decrease of the inward pinch with increasing collisionality but already at much smaller values of the collisionality the pinch change sign from inward to outward [41,53]. The gyro-kinetic simulations in fact suggest that the density profile should always be flat, in contrast to the observations. Since the GLF model is based on a moment approach of the gyro-kinetic equations, the latter are more trust worthy from a theoretical point of view, in the case of a disagreement.

Collisionality also plays an important role in the competition between the different instabilities since it weakens the TEM but not the ITG. In H-mode plasmas with dominant ion heating the dominant instability is usually the ITG. Only at lower density the TEM can become dominant because of the higher density gradient but also because of the lower collisionality [56].

7.3. Electro-magnetic effect

For all electrostatic models the results are independent of the plasma β. This parameter enters when the electromagnetic effects, usually in the form of only the parallel component of the vector potential ($A_\parallel$), are kept. Almost all of the models are able to retain this effect, but it is often not switched on in the modelling, or its effects are not separately discussed. Therefore, all the implications of the finite beta values, and how well the models describe the finite beta effects are not well known.

It is known that an increase in beta stabilises the ITG. Modelling with GLF23 has revealed that the model predicts a somewhat to strong beta scaling [59]. The electromagnetic effects lead to a non-adiabatic electron response and consequently can influence the particle flux. Studies of this effect [61] however, seem to yield relatively weak effects.

8. ITER projections

As already stated in the introduction the accuracy of the transport models is not expected to be sufficient to come to completely reliable ITER prediction. Furthermore, the models describe only the inner part of the plasma, they need a boundary condition at 80 or 90% of the plasma radius. The threshold of the instabilities combined with the stiffness of the profiles makes that the plasma stored energy is very sensitive (i.e., almost linearly related) to the edge temperature. The latter is especially true for the IFS-PPPL and the GLF23 model. The Weiland and Multi-mode model [12] show a somewhat weaker dependence due to the weaker stiffness, and their prediction of the fusion gain is more optimistic [8, 60]. It appears though that nonlinear simulations (although maybe not as stiff as IFS-PPPL) predict a profile stiffer than the Weiland/MMM.

Several models (empirical and semi-empirical) exist to predict the edge temperature in ITER. The predictions however vary in the range 1–5 keV and do not provide for a reasonably accurate value. The best one can do at present is to predict the fusion gain Q as a function of the pedestal temperature for each model. This exercise has been done by different authors and groups [8,40,60,62], with the outcome that one most probably needs a relatively large pedestal temperature $T_{\mathrm{ped}} > 3$ keV.

Most of the simulations for ITER have been done for fixed flat density profiles. The GLF23 model, however, predicts a moderately peaked density profile in good agreement with current experiments. Such a peaking of the density could lead to a 30% increase in the fusion gain at constant volume averaged density [63]. However, as already discussed, the predictions of this model are in disagreement with the more complete gyro-kinetic theory. At present there is, therefore, no good theoretical prediction of the observed density peaking. However, in this model the collisions have a weaker influence compared with gyro-kinetic simulations. The latter appear to predict a flat profile even at the collisionality values of ITER. Of course the gyro-kinetic simulations (linear or non-linear) can not predict current experiments correctly in this point, which makes that it is still unclear what the exact shaper of the density profile in ITER will be.

9. Conclusions

In this article a short introduction into transport models and their main properties is given. The reliability of the models is limited but it appears that several observations can be well explained with them. They remain to have limited predictable capability since they are unable to model the H-mode barrier properly, and one therefore needs to assume a boundary condition at 80 or 90% of the plasma radius. Unfortunately the threshold of the modes and the stiffness of the profile make that the predictions are sensitive to the assumed value. For ITER one finds that $Q = 10$ will require a reasonably high edge temperature $3 < T_{\mathrm{ped}} < 5$ keV. Pedestal models are not in disagreement with such a value but an accurate prediction is unfortunately not possible.

References

[1] M. Kotschenreuther, et al., Phys. Plasmas 2 (1995) 2381.
[2] T. Dannert, F. Jenko, Phys. Plasmas 12 (2005), Art. No. 072309.
[3] B.D. Scott, Phys. Rev. Lett. 65 (1990) 3289.
[4] R.E. Waltz, R.L. Miller, Phys. Plasmas 6 (1999) 4265.
[5] J. Anderson, H. Nordman, J. Weiland, Plasma Phys. Control. Fusion 42 (2000) 545.

[6] J. Anderson, H. Nordman, J. Weiland, Phys. Plasmas 8 (2001) 180.
[7] K. Itoh, S.-I. Itoh, A. Fukuyama, et al., Plasma Phys. Control. Fusion 36 (1994) 279.
[8] M. Wakatani, V.S. Mukhovatov, K.H. Burrell, et al., Nucl. Fusion 39 (1999) 2175.
[9] J. Weiland, A.B. Jarmen, H. Nordman, Nucl. Fusion 29 (1989) 1810.
[10] H. Nordman, J. Weiland, A. Jarmen, Nucl. Fusion 30 (1990) 983.
[11] J. Weiland, Collective Modes in Inhomogeneous Plasmas, Institute of Physics Publ., Bristol, 2000.
[12] G. Bateman, A.H. Kritz, J.E. Kinsley, et al., Phys. Plasmas 5 (1998) 1793.
[13] J.E. Kinsey, G. Bateman, Phys. Plasmas 3 (1996) 3344.
[14] R.E. Waltz, G.M. Staebler, W. Dorland, et al., Phys. Plasmas 4 (1997) 2482.
[15] M. Kotschenreuther, G. Rewoldt, W.M. Tang, Comput. Phys. Commun. 88 (1995) 128.
[16] J.E. Kinsey, Fusion Sci. Tech. 48 (2005) 1060.
[17] J. Candy, R.E. Waltz, J. Comput. Phys. 186 (2003) 545.
[18] C. Bourdelle, X. Garbet, G.T. Hoang, et al., Nucl. Fusion 42 (2002) 892.
[19] G. Rewoldt, M.A. Beer, M.S. Chance, et al., Phys. Plasmas 5 (1998) 1815.
[20] S. Brunner, M. Fivaz, T.M. Tran, et al., Phys. Plasmas 5 (1998) 3929.
[21] G.L. Falchetto, J. Vaclavik, L. Villard, Phys. Plasmas 10 (2003) 1424.
[22] R.E. Waltz, G.D. Kerbel, J. Milovich, Phys. Plasmas 1 (1994) 2229.
[23] T.S. Hahm, K.H. Burrell, Phys. Plasmas 2 (1995) 1648.
[24] T. Tala, X. Garbet, JET EFDA contributors, Physics of Internal Transport Barriers, C. R. Physique 7 (2006), this issue.
[25] C.C. Petty, J.E. Kinsey, T.C. Luce, Phys. Plasmas 11 (2004) 1011.
[26] G. Tardini, A.G. Peeters, et al., Nucl. Fusion 42 (2002) L11.
[27] J.C. DeBoo, J.E. Kinsey, R. Bravenec, et al., Nucl. Fusion 39 (1999) 1935.
[28] G. Tardini, et al., Nucl. Fusion 42 (2002) 258.
[29] A.G. Peeters, C. Angioni, M. Apostoliceanu, et al., Phys. Plasmas 12 (February 2005), Art. No. 022505.
[30] F. Ryter, G. Tardini, F. De Luca, et al., Nucl. Fusion 43 (2003) 1396.
[31] F. Ryter, C. Angioni, A.G. Peeters, et al., Phys. Rev. Lett. (2005), Art. No. 085001.
[32] F. Jenko, T. Dannert, C. Angioni, Plasma Phys. Control. Fusion 47 (2005) B195.
[33] J.C. DeBoo, S. Cirant, T.C. Luce, et al., Nucl. Fusion 45 (2005) 494.
[34] G.T. Hoang, Phys. Rev. Lett. 87 (2001), Art. No. 125001.
[35] W. Horton, G.T. Hoang, C. Bourdelle, Phys. Plasmas 11 (2004) 2600.
[36] P. Mantica, F. Ryter, C. R. Physique 7 (2006), this issue.
[37] A.G. Peeters, et al., Nucl. Fusion 42 (2002) 1376.
[38] R.C. Wolf, Y. Baranov, X. Garbet, et al., Plasma Phys. Control. Fusion 45 (2003) 1757.
[39] A.B. Dimits, B.I. Cohen, N. Mattor, et al., Nucl. Fusion 40 (2000) 661.
[40] A.M. Dimits, G. Bateman, M.A. Beer, et al., Phys. Plasmas 7 (2000) 969.
[41] C. Estrada-Mila, J. Candy, R.E. Waltz, Phys. Plasmas 12 (2005), Art. No. 022305.
[42] X. Garbet, N. Dubuit, E. Asp, Y. Sarazin, C. Bourdelle, et al., Phys. Plasmas 12 (2005), Art. No. 082511.
[43] J. Weiland, H. Nordman, Phys. Fluids B 5 (1993) 1669.
[44] B. Coppi, C. Spight, Phys. Rev. Lett. 41 (1978) 551.
[45] C. Angioni, A.G. Peeters, Direction of impurity pinch and auxiliary heating in tokamak plasmas, Phys. Rev. Lett. 96 (2006), Art. No. 095003.
[46] X. Garbet, R.E. Waltz, Phys. Plasmas 3 (1996) 1898.
[47] R.E. Waltz, Fusion Sci. Tech. 48 (2005) 1051.
[48] P. Strand, H. Nordman, J. Weiland, J.P. Christiansen, Nucl. Fusion 38 (1998) 545.
[49] H. Nordman, P. Strand, J. Weiland, J.P. Christiansen, Nucl. Fusion 37 (1997) 413.
[50] C. Angioni, A.G. Peeters, G.V. Pereverzev, et al., Phys. Plasmas 10 (2003) 3225.
[51] C. Angioni, A.G. Peeters, G.V. Pereverzev, et al., Phys. Rev. Lett. 90 (2003), Art. No. 205003.
[52] H. Weisen, A. Zabolotsky, C. Angioni, Nucl. Fusion 45 (2005) L1.
[53] C. Angioni, A.G. Peeters, F. Jenko, et al., Phys. Plasmas 12 (2005), Art. No. 112310.
[54] X. Garbet, L. Garzotti, P. Mantica, et al., Phys. Rev. Lett. 91 (2003), Art. No. 035001.
[55] C. Angioni, A.G. Peeters, F. Ryter, et al., Phys. Plasmas 12 (2005), Art. No. 040701.
[56] C. Angioni, A.G. Peeters, X. Garbet, et al., Nucl. Fusion 44 (2004) 827.
[57] N. Mattor, P.H. Diamond, Phys. Fluids 31 (1988) 1180.
[58] A.G. Peeters, C. Angioni, Phys. Plasmas 12 (2005), Art. No. 072515.
[59] J.E. Kinsey, Nucl. Fusion 39 (1999) 539.
[60] J.E. Kinsey, G. Bateman, T. Onjun, et al., Nucl. Fusion 43 (2003) 1845.
[61] A. Eriksson, J. Weiland, Phys. Plasmas 12 (2005), Art. No. 092509.
[62] V. Mukhovatov, Y. Shimomura, A. Polevoi, et al., Nucl. Fusion 43 (2003) 942.
[63] G.V. Pereverzev, C. Angioni, A.G. Peeters, et al., Nucl. Fusion 45 (2005) 221.